(60°); $Q_1=-1.03(7)$ (0°), $-1.03(9)$ Mev (60°). And while the absolute accuracy of the $Q$ values is not very high because of the uncertainty in the incident $He^3$ energy, the excitation energy of the excited state is well determined: $E_x=0.995\pm0.04$ Mev (the error given arises from the uncertainty in the $t_c$ value). This excitation energy is consistent with the energy (1.274 Mev) of the first excited state in $Ne^{22}$. The $Q_0$ and $Q_1$ values are estimated to be $-0.04\pm0.08$ and $-1.04\pm0.08$ Mev. The $Q_0$ value leads to a mass excess $(M-A)$ for $Mg^{22}=-0.14\pm0.08$ Mev (based on $C^{12}$, and on the Mattauch-Wapstra masses[12] for $Ne^{20}$, $He^3$, and $n$). The lowest particle binding energy in $Mg^{22}$ is then 5.22 Mev for $(Na^{21}+p)$.

The relative yields of the 0 and 1 groups are consistent with their presumably $J=0^+$ and $2^+$ character. Group 1 should become relatively stronger at 60°. An extremely rough calculation of the differential cross section at 0° of the ground-state group suggests 0.5 mb/sr. This is a reasonable value for a $(He^3,n)$ group.[28]

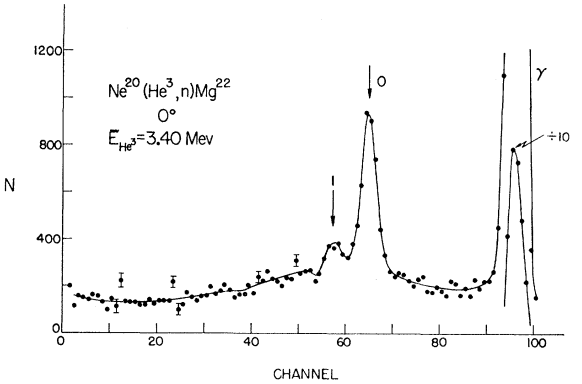


FIG. 19. The time spectrum of neutrons from the $Ne^{20}(He^3,n)Mg^{22}$ reaction for an incident energy of 3.40 Mev, as seen at 0° to the incident $He^3$ beam. The peak labeled 0 corresponds to the ground state of $Mg^{22}$, that labeled 1 to the state at 0.995 Mev. The flight path was 1.97 m.

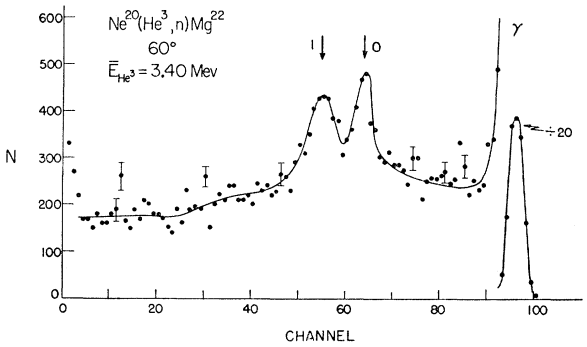


FIG. 20. The data at 60°, $\bar{E}(He^3)=3.40$ Mev (see also caption of Fig. 19).

This experiment is obviously a very preliminary one. One of us (F.A.S.) plans to repeat it in the near future. It is reported here only because of the complete lack of experimental information on $Mg^{22}$.


## ACKNOWLEDGMENTS

We are very grateful to the staff of the P-9 group, and in particular to Dr. J. S. Levin and to Mrs. Dana Douglass, for their valuable assistance. We are much indebted also to Dr. J. L. McKibben for the design and construction of the terminal pulser used in this work. It is a pleasure to thank Dr. L. S. Rodberg and Professor W. Selove for their very helpful comments on the analysis of the data. One of us (F.A.S.) wishes to express her deep appreciation to the Los Alamos Scientific Laboratory for a thoroughly enjoyable and interesting sojourn.


[28] D. A. Bromley and E. Almqvist, *Reports on Progress in Physics* (The Physical Society, London, 1959), Vol. 23, p. 544.

PHYSICAL REVIEW VOLUME 124, NUMBER 5 DECEMBER 1, 1961

# Excitation Functions of $K^{41}+p$ Reactions*

R. D. SHARP, L. F. CHASE, JR., R. M. FRIEDMAN,† E. K. WARBURTON,‡ AND E. G. SHELLEY
*Research Laboratory, Lockheed Missiles and Space Company, Sunnyvale, California*

(Received July 12, 1961)

The energy of some of the gamma radiation following the proton bombardment of $K^{41}$ has been measured, and the origins of some of these gamma rays have been determined. The excitation functions of the 1.00-Mev gamma from inelastic scattering in $K^{41}$ and the 2.16-Mev gamma from the $K^{41}(p,\alpha\gamma)$ reaction have been measured in a region between 2.3 and 3.5 Mev and approximately 50 resonances observed. The energies and absolute cross sections, and the anisotropy of the gamma radiation proceeding from some of these resonances have been measured, leading to information on the excited states in $Ca^{42}$ at about 13-Mev excitation, including an upper limit on the average level spacing. Evidence is given to show the 100-Mev level in $K^{41}$ is most likely a $\frac{1}{2}+$ state in agreement with theoretical predictions.

## INTRODUCTION

THE low-lying states of nuclei near the doubly magic $Ca^{40}$ are of particular interest from the point of view of the $jj$-coupling shell model. Recent theoretical analyses have yielded results in good agreement with experiment,[1–3] while other specific predic-

* Supported by the joint program of the U. S. Atomic Energy Commission and the Lockheed General Research Program.

† Now at Aerospace Corporation, El Segundo, California.

‡ Permanent Address: Physics Department, Princeton University, Princeton, New Jersey.

[1] C. Levinson and K. W. Ford, Phys. Rev. **99**, 792 (1955); **100**, 11 (1955).

[2] J. B. French and B. J. Raz, Phys. Rev. **104**, 1411 (1956).

[3] S. P. Pandya, Progr. Theoret. Phys. (Kyoto) **19**, 404 (1958).

tions, including some on $K^{41}$, remain to be checked experimentally. In particular, Pandya[3] calculates the positions of the excited states of the $(d_{3/2})^{-1}(f_{7/2})^2$ configuration in $K^{41}$. He obtains energies of 1.0, 2.1, 2.2, and 1.8 Mev for the states of spin $\frac{1}{2}$, $\frac{3}{2}$, $\frac{5}{2}$, and $\frac{7}{2}$, respectively.

At high excitation energies, the average properties of levels are at present all that can be compared with theoretical predictions. Observations of the level density can be compared with the semi-empirical models based primarily on data obtained from slow neutron initiated reactions.[4,5] These observations are especially valuable if experimental information can be obtained on the distribution of spins among the states. Measurements of the distribution of partial reaction widths have been interpreted by Porter and Thomas and others.[6,7] The average values of the reaction cross section can provide information about the relevant strength functions[8] which have been predicted theoretically by the optical model[9] and the independent-particle model.[10]

This paper presents information on the low-lying states of $K^{41}$ and the higher excited states of $Ca^{42}$ which were obtained from experiments involving the proton bombardment of $K^{41}$.[11] At the time that these experiments were initiated, very little was known about either the low-lying states of $K^{41}$ or the higher excited states of $Ca^{42}$. More recently, experimental work by Enge *et al.*[12] and by Clarke, *et al.*[13] has yielded information about both these nuclei. Where comparable, these results are in agreement with those reported here.

## EXPERIMENTAL OBSERVATIONS

### Identification of Gamma Radiation

A preliminary study of the gamma radiation following the proton bombardment of natural potassium targets revealed several prominent gamma rays with energies less than 3 Mev. Thick targets of various potassium compounds of natural isotopic abundance (93.2%$K^{39}$ and 6.8%$K^{41}$) were bombarded with protons of energies up to 3.3 Mev from the Lockheed electrostatic accelerator, and the resulting spectra of gamma radiation were studied to determine which of the observed gamma rays originated in the potassium nuclei.

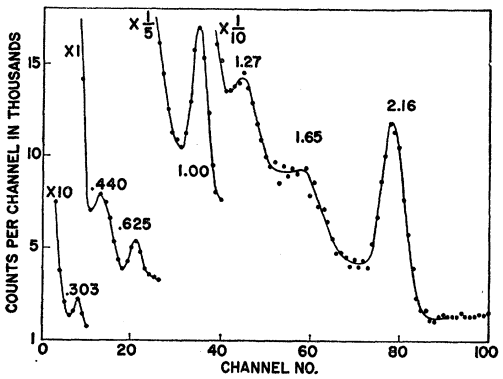


FIG. 1. A typical gamma-ray spectrum from the proton bombardment of a thin natural KI target on a tantalum backing. The gamma-ray energies in Mev are listed near the total absorption peaks. The incident energy was 3.04 Mev, and the exposure length was 214 microcoulombs.

The radiation was observed with a 4-in. by 4-in. NaI crystal scintillation spectrometer. The instrument was mounted on a carriage which could be rotated around the target through an arc of 240° and set at any distance between 1 and 12 in. from the target. Energy analysis of the pulses from the spectrometer was performed with the aid of a 100-channel analyzer. A typical spectrum is shown in Fig. 1.

The energies of the observed gamma rays were determined by calibration of the spectrometer with various radioactive sources whose gamma-ray energies are well known. Table I lists the sources used and the resulting energies of the potassium gamma radiation. The values of the energies shown are accurate to within ±1% for the 1.00- and 2.16-Mev radiation and within ±3% for the less prominent 1.27-Mev radiation. The gamma-ray

TABLE I. Energy determination of gamma radiation.

| Calibration gamma radiation Energy (Mev) | Source |
|---|---|
| 0.279 | $Hg^{203}$ |
| 0.303 | $Ta^{a}$ |
| 0.511 | $Na^{22}$ |
| 0.662 | $Ca^{137}$ |
| 1.277 | $Na^{22}$ |
| 1.48 | $Pr^{144}$ |
| 2.18 | $Pr^{144}$ |
| 2.614 | $Th^{232}$ |
| **Gammas observed from proton bombardment of KI Energy (Mev)** | |
| 0.440±0.010 | |
| 0.625±0.010 | |
| 1.00 ±0.010 | |
| 1.27 ±0.030 | |
| 1.65[b] | |
| 2.16 ±0.020 | |

[a] Coulomb excitation of tantalum target backing.
[b] Several unresolved groups centered at this energy including first escape peak of 2.16-Mev gamma.

[4] T. D. Newton, Can. J. Phys. **34**, 804 (1956). See also expression by H. Feshbach, in *Nuclear Spectroscopy*, edited by F. Ajzenberg-Selove (Academic Press, Inc., New York, 1960), Part B, p. 668.
[5] A. G. W. Cameron, Can. J. Phys. **35**, 1021 (1957); **36**, 1040 (1958); **37**, 244 (1959).
[6] C. E. Porter and R. G. Thomas, Phys. Rev. **104**, 483 (1956).
[7] See review by J. A. Harvey, in *Proceedings of the International Conference on Nuclear Structure, Kingston* (University of Toronto Press, Toronto, 1960), Chap. 71, p. 659.
[8] J. P. Schiffer and L. L. Jee, Jr., Phys. Rev. **109**, 2099 (1958).
[9] H. Feshbach, C. E. Porter, and V. F. Weisskopf, Phys. Rev. **96**, 448 (1954).
[10] A. M. Lane, R. G. Thomas, and E. P. Wigner, Phys. Rev. **98**, 693 (1955).
[11] R. D. Sharp, R. M. Friedman, and L. F. Chase, Jr., Bull. Am. Phys. Soc. **3**, 419 (1958); **4**, 366 (1959); R. D. Sharp, L. F. Chase, Jr., E. K. Warburton, and R. M. Friedman, *ibid.* **6**, 46 (1961).
[12] H. A. Enge, W. H. Moore, and J. W. Kelley, Bull. Am. Phys. Soc. **3**, 210 (1958).
[13] R. L. Clarke, E. Almqvist, and E. B. Paul, Nuclear Phys. **14**, 472 (1959).

peak centered at 1.65 Mev was considerably broadened and appeared to arise from two or more unresolved levels. In addition, there is higher energy gamma radiation of comparatively low yield, whose energy was not well determined.

As a further step in establishing the origin of the observed gamma rays, a series of gamma-gamma coincidence measurements was made, utilizing a second 4-in. by 4-in. NaI spectrometer in conjunction with the one previously described. Targets of natural potassium metal and of potassium iodide enriched to 86.8% in $K^{41}$ were used. Conventional fast-slow coincidence circuitry was employed with a nominal 30 mμsec resolving time in the fast circuit. Differential gates were set around the photopeaks of the various low-energy gamma rays, and the coincidence spectra were observed. Gamma radiation of $1.55\pm0.03$ and $0.52\pm0.03$ Mev were observed in all the coincidence spectra. It was concluded that these two observed gamma rays were in coincidence with higher energy gamma radiation whose Compton tails fell within the differential gates. This is consistent with the expected $(p,\gamma)$ cascades through the first-excited states of $Ca^{42}$ and $Ca^{40}$ from $K^{41}(p,\gamma)$ and $K^{39}(p,\gamma)$ reactions, respectively. The first excited state of $Ca^{42}$ is at 1.52 Mev. The first excited states of $Ca^{40}$ at 3.35 Mev is $0+$ and decays by pair production, giving rise to 0.511-Mev annihilation radiation. Some of the observed annihilation radiation also arises from pair production by high-energy gammas in coincidence with other high-energy gammas in the cascade transitions of both $Ca^{40}$ and $Ca^{42}$. No coincidences were observed which were attributable to gamma radiation in coincidence with the photopeaks in question.

Since these low-energy gamma rays are not in coincidence with other gamma radiation, they cannot originate from a $(p,\gamma)$ process. To determine if they arise from $(p,p')$, $(p,\alpha)$, or $(p,d)$ reactions, charged particle-gamma ray coincidence experiments were performed with both natural and enriched targets. A 1-in.-diam CsI crystal was hand-polished to approximately 0.007-in. thickness and cemented directly to the face of a 6655 photomultiplier. A thin layer of aluminum was then evaporated onto the crystal and photomultiplier face to act as a light shield and as a reflector. The unit was positioned inside the vacuum system at 150° with respect to the incident proton beam direction, to minimize the background of elastically scattered particles. A diaphragm with a $\frac{1}{2}$-in. aperture was placed in front of the crystal to improve the resolution of the system. The thickness of the aluminum layer on the crystal was determined by measuring the half-width of the $Al^{27}(p\gamma)$ resonance at 991 kev from an aluminum layer deposited during the evaporation on a glass slide next to the phototube. The unit was calibrated with a $Po^{210}$ source (5.3-Mev alpha particles) made by dipping a 0.010-in. silver wire in a polonium chloride solution. This source was mounted in the target chamber at the position of the beam spot and gave rise to a peak of 7% resolution

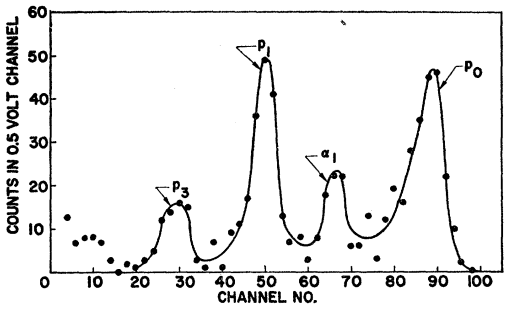


FIG. 2. The spectrum of protons and alpha particles in coincidence with gamma radiation between 0.6 and 1.3 Mev. The incident proton energy was 3.04 Mev, and the exposure length was 500 microcoulombs. The peaks have been identified as follows: $p_0$=chance coincidence peak from elastic scattering, primarily from the gold and iodine in the target. $\alpha_1$=alpha-particle group from the $K^{41}(p,\alpha\gamma)$ reaction to the 2.16-Mev state in $Ar^{38}$, in coincidence with Compton scattered gamma radiation in the energy region studied. $p_1$=proton group from the $K^{41}(p,p'\gamma)$ reaction to the 1.00-Mev state in $K^{41}$ in coincidence with the total absorption peak at 1.00 Mev. $p_3$=proton groups from the $K^{41}(p,p'\gamma)$ reaction to four excited states near 1.65 Mev in $K^{41}$, in coincidence with Compton-scattered gamma radiation in the energy region studied.

(full width at half-maximum divided by peak energy). The apparatus was tested using the alpha-particle groups from the $F^{19}(p,\alpha\gamma)$ reaction which are in coincidence with gamma-ray groups of energies from 6 to 7 Mev.

The CsI spectrometer was used to observe the charged particles in coincidence with the various low-energy gamma rays from potassium. Thin targets were prepared by evaporating potassium iodide onto backings, consisting of a thin film of Formvar onto which a thin layer of gold had previously been evaporated.

Long coincidence runs were made with the incident beam currents held to less than 0.03 μa to minimize the chance coincidence background. The charged-particle spectra in coincidence with the various gamma rays are shown in Figs. 2–4. The results of the experiments are summarized in Table II. They are consistent with the 2.16-Mev gamma ray originating from the $K^{41}(p,\alpha\gamma)$ reaction to a known level in $Ar^{38}$ and the 1.00-Mev

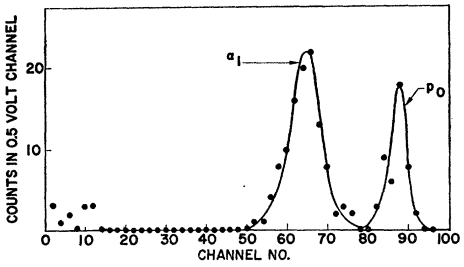


FIG. 3. Alpha particles in coincidence with gamma radiation between 2.0 and 2.3 Mev. The incident proton energy was 3.04 Mev, and the exposure length was 600 microcoulombs. The peaks have been identified as follows: $p_0$=chance coincidence peak from elastic scattering. $\alpha_1$=alpha-particle group from the $K^{41}(p,\alpha\gamma)$ reaction to the 2.16-Mev state in $Ar^{38}$, in coincidence with the total absorption peak at 2.16 Mev.

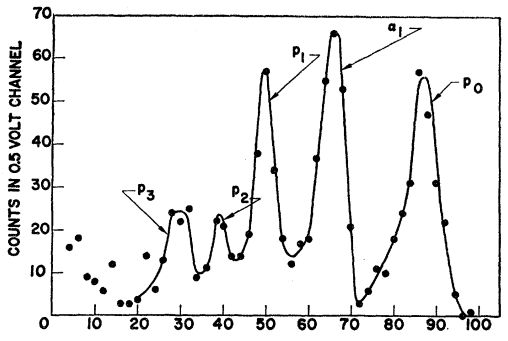


FIG. 4. Spectrum of protons and alpha particle in coincidence with gamma radiations of energy greater than 0.8 Mev. The incident proton energy was 3.04 Mev, and the exposure length was 520 microcoulombs. The peaks have been identified as follows: $p_0$=chance coincidence peak from elastic scattering $\alpha_1$=alpha-particle group from $K^{41}(p,\alpha\gamma)$ reaction to the 2.16-Mev state in $Ar^{38}$. $p_1-p_3$=proton groups from inelastic scattering in $K^{41}$ to the 1.00- and 1.27-Mev levels, and to an unresolved group of levels near 1.6 Mev.

gamma ray, and the 1.27- and 1.65-Mev gamma rays arising from inelastic proton scattering. The origins of the 0.440- and 0.625-Mev gamma rays have not yet been established.

These results are consistent with some recent findings by Enge *et al.*, using a magnetic spectrograph and enriched isotopic targets.[12] In a study of inelastic proton scattering at 7-Mev incident energy, they found energy levels in $K^{41}$ at 0.99 and 1.30 Mev, and were able to resolve the group at 1.65 Mev into four components of 1.57, 1.59, 1.69, and 1.71 Mev. They also saw levels at 2.15 and 2.17 Mev which were not appreciably excited at our lower bombarding energies.

## Excitation Functions

The excitation functions of the two most prominent of the gamma rays were measured over the range from 2.3 to 3.5 Mev. Preliminary studies were made with targets of natural isotopic abundance which were approximately 50-kev thick to the incident proton beam. Potassium metal targets were prepared by evaporation onto tantalum backings directly in the target chamber, since even a brief exposure to air completely oxidizes them. Targets of potassium iodide evaporated onto tantalum backings were also used, and proved to be preferable, having less contaminant content. The results from both varieties of targets were in agreement.

TABLE II. Results of charged particles-gamma ray coincidence experiments proton bombardment of KI (natural isotopic abundance). Bombarding energy=3.04 Mev.

| Particle observed | Particle energy observed (Mev) | Reaction | State in final nucleus (Mev) | Particle energy expected from a reaction to this final state (Mev) |
|---|---|---|---|---|
| Proton | 1.23 (av) | $K^{41}(p,p')$ | 1.51–1.71 | 1.23 (av) |
| Proton | 1.50 | $K^{41}(p,p')$ | 1.30 | 1.55 |
| Proton | 1.83 | $K^{41}(p,p')$ | 1.00 | 1.85 |
| Alpha | 4.02 | $K^{41}(p,\alpha)$ | 2.15 | 4.12 |

The targets were bombarded with protons of energies between 2.0 and 3.5 Mev in 10- to 20-kev steps. Points were taken systematically varying the incident proton energy in both increasing and decreasing directions. Frequent repetitions were made to detect any changes in the target or the detection apparatus. A cold trap which was placed approximately $\frac{1}{8}$ in. from the target was maintained at liquid nitrogen temperature throughout the bombardment.

The length of the exposure at each data point was determined by integrating the beam current entering the target chamber, which was insulated from the rest of the vacuum system and appropriately biased to minimize the emission of secondary electrons. In addition, the 303-kev Coulomb excitation gamma ray from the tantalum backing was monitored, separately, with a single-channel analyzer. Its excitation function was observed to be a smoothly varying, almost linear, curve in agreement with expectations, and served as a check on the current integrating procedure used in the experiment.

TABLE III. Calibration points used for analyzing magnet and a comparison of the energies of prominent resonances observed with both the natural targets of 50-kev half-width and the enriched targets of 15-kev half-width.

| Energy calibration points for analyzing magnet | | | |
|---|---|---|---|
| Calibration energy | | Resonance energy | |
| (Mev) | Reaction | (Mev) | Beam |
| 0.8724 | $F^{19}(p,\alpha\gamma)$ | 0.8724 | $H^+$ |
| 0.9924 | $Al^{27}(p\gamma)$ | 0.9924 | $H^+$ |
| 1.7476 | $C^{13}(p\gamma)$ | 1.7476 | $H^+$ |
| 3.4896 | $F^{19}(p,\alpha\gamma)$ | 0.8724 | $H_2^+$ |
| 3.9696 | $Al^{27}(p\gamma)$ | 9.9924 | $H_2^+$ |

| Prominent resonances in excitation functions | | |
|---|---|---|
| | Resonance energy (Mev) corrected for target thickness | |
| Reaction | Natural targets | Enriched targets |
| $K^{41}(p,p'\gamma)$ 1.00-Mev gamma | 2.51 | 2.507 |
| | 3.02 | 3.018 |
| | 3.14 | 3.142 |
| | 3.20[a] | 3.176, 3.195, 3.225 |
| | 3.29 | 3.300 |
| | 3.41 | 3.414 |
| $K^{41}(p,\alpha\gamma)$ 2.16-Mev gamma | 3.02[a] | 2.996, 3.018 |

[a] Unresolved group.

The entire gamma-ray spectrum up to 2.5 Mev was recorded at each energy by the 100-channel analyzer. Only the two most prominent gamma rays have been analyzed in detail. The excitation functions of these, the 1.00- and 2.16-Mev gammas, exhibited several partially resolved resonances (Table III), and it was decided to repeat the experiments with thinner targets enriched in $K^{41}$. A target approximately 15-kev thick was prepared of KI enriched to 86.8% in $K^{41}$. It also

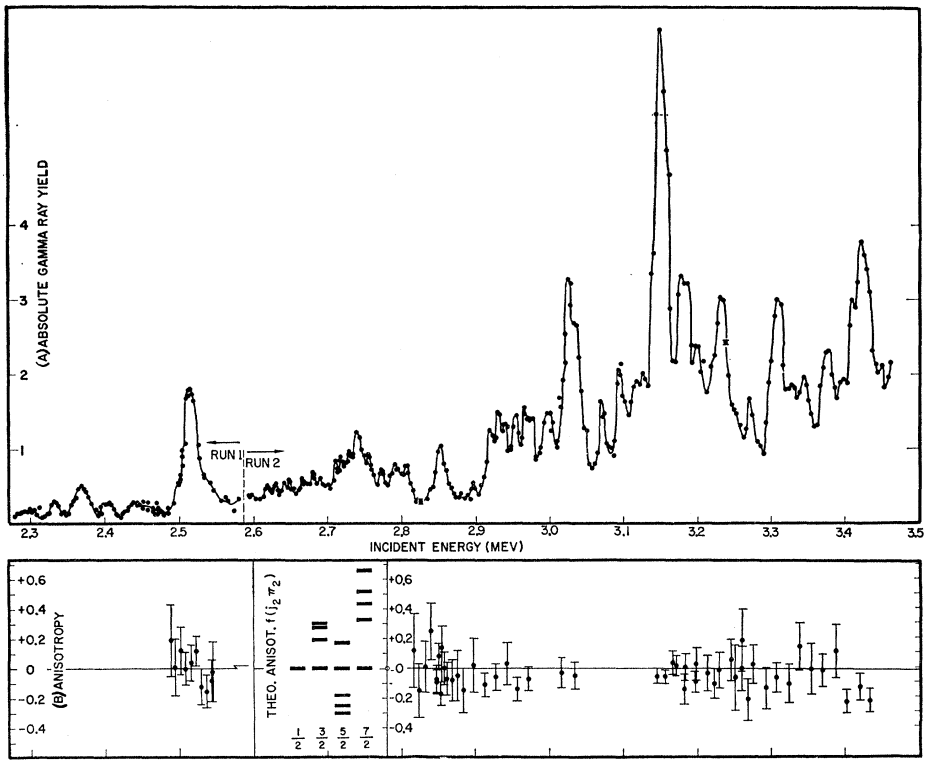


FIG. 5. (a) Excitation function of 1.00-Mev gamma radiation. The absolute yields are given as follows: Run 1—One scale unit equals $29\times10^{-10}$ gamma ray per incident proton. Run 2—One scale unit equals $33\times10^{-10}$ gamma ray per incident proton. (b) Measured and calculated anisotropies. See Table VI and text for assumptions made in calculations and definitions of terms.

was made by vacuum evaporation onto a tantalum backing. The excitation function was measured as described above, except that it was studied in greater detail. Over 500 exposures were made at approximately 3-kev intervals from 2.2 to 3.5 Mev. Each section of the yield curve was gone over at least twice, both for increasing and decreasing beam energy. Frequent repetitions were made and the reproducibility of the data was excellent. The effects of any carbon buildup on the target were checked by repeatedly tracing out the front edge of a particularly large resonance at intervals during the course of the experiment and observing that any energy degradation of the beam was negligible.

The excitations functions obtained with the enriched targets are shown in Fig. 5(a) for the 1.00-Mev gammas and Fig. 6(a) for the 2.16-Mev gammas. For clarity, some of the data points have been omitted in the region of overlap between runs 1 and 2 (2.5 to 2.75 Mev). In the region above 3.25 Mev, the 2.16-Mev gamma ray was obscured by 1.95-Mev radiations from the $K^{41}(p,n\gamma)$ and $K^{39}(p,\alpha\gamma)$ reactions. The thinner targets and higher yields brought out considerable structure which was not

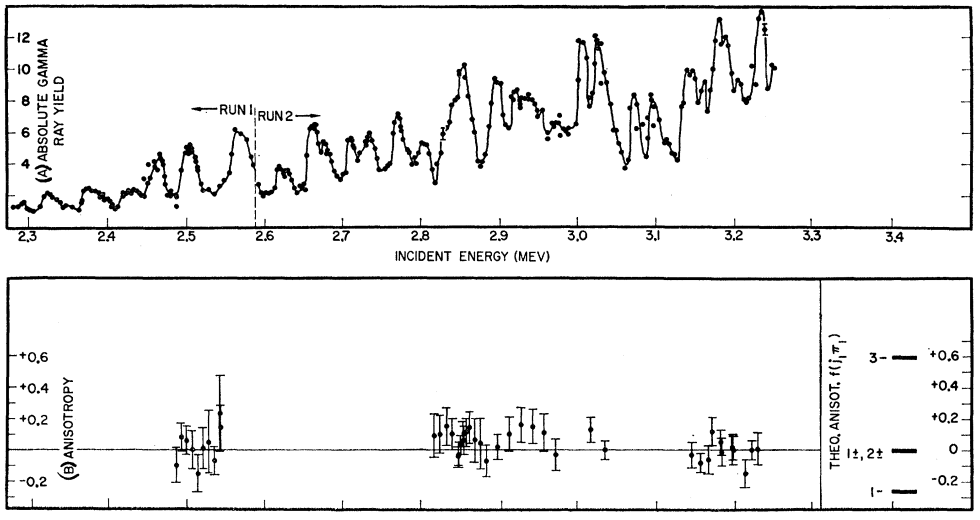


FIG. 6. (a) Excitation function of 2.16-Mev gamma radiation. The absolute yields are given as follows: Run 1—One scale unit equals $6.5\times10^{-10}$ gamma ray per incident proton. Run 2—One scale unit equals $7.5\times10^{-10}$ gamma ray per incident proton. (b) Measured and calculated anisotropies. See Table VI and text for assumptions made in calculations and definitions of terms.

observed in the preliminary experiments. However, the gross features of the excitation function reproduced satisfactorily those results obtained with the natural targets.

A precise energy calibration of the beam-analyzing magnet was made to determine accurately the energies of the resonances in the various excitation curves. Some calibration points were taken both before and after each run, and the calibration constant was observed to be the same. In Table III are listed the well-known nuclear reactions used as calibration points, and the corresponding energies of the most prominent resonances in the excitation functions obtained with both the nautral and enriched targets. The widths of the observed resonances were assumed to be due primarily to target thickness and the corresponding correction of one-half this amount has been applied.

The cross-section measurements were made absolute by determining the photopeak efficiency of the NaI crystal spectrometer in the geometry of the experiment with a calibrated source of $Na^{24}$.[14] Two points on the efficiency curve at 1.37 and 2.75 Mev gamma-ray energy were thus obtained and were used to normalize efficiency curves of the correct shape for a 4-in. by 4-in. NaI crystal.[15] The estimated precision of the absolute cross-section scale shown on Figs. 5 and 6 is $\pm 25\%$.

The target thickness was determined by elastically scattering protons from the tantalum-backed target and from a clean piece of tantalum. The difference in the energy of the scattered protons was observed with our new broad-range magnetic spectrograph. An energy difference ($\Delta E$) corresponding to twice the target thickness is obtained both from the relative displacement of the step function due to protons scattered from tantalum and from the width of the peak due to protons scattered from the iodine in the KI of the target material. This latter peak was not completely resolved from the tantalum step. It was graphically separated using the above condition on $\Delta E$. A target thickness of 15 kev to 3-Mev protons in the geometry of the excitation function experiments was obtained.

## Anisotropy Measurements

The region of the previously observed excitation curve containing the most pronounced structure was repeated, using as detectors, two 4-in. by 4-in. NaI crystal spectrometers set at 0° and 90° to the incident beam direction. The pulses from each detector were fed into separate 100-channel analyzers. Three-inch-thick Pb collimators were used to cut down the low-energy background and approximately match the counting rates in the two detectors; thereby, making the dead-time corrections to the derived anisotropy negligible. The incident beam energy was calibrated at 1.747 Mev with the $C^{13}(p,\gamma)N^{14}$ reaction and with the previously observed resonances in the gamma radiation from the $K^{41}$ target.

TABLE IV. Measured asymmetries. A comparison of the instrumental asymmetry as measured with a $Na^{24}$ source and the rms asymmetry for each gamma ray averaged over all resonances studied.

| Gamma radiation | $[W(90°)/W(0°)]$ rms |
|---|---|
| 1.00 Mev | $0.851\pm0.014$ |
| 2.16 Mev | $0.806\pm0.013$ |
| $Na^{24}$ | $0.845\pm0.020$ |

The instrumental anisotropy for gamma radiation emitted at the position of the beam spot was measured by inserting a NaBr target in the target chamber and bombarding it with deuterons, thereby producing $Na^{24}$ with a 15-hr half-life. Following the bombardment the photopeak yields of the 2.75 and 1.37 Mev gamma rays from this isotope were compared at 0° and 90°, and the measured $K^{41}$ gamma-ray anisotropies were corrected by the observed ratio.

The observed anisotropy in the gamma radiation from the $K^{41}$ target is shown in Figs. 5(b) and 6(b). The anisotropy is defined as $[W(0°)-W(90°)]/W(90°)$ where $W(\theta)$ is the integrated photopeak yield at the angle $\theta$ to the incident beam. A smooth background was subtracted from the photopeaks. The errors indicated are statistical, plus an estimate of the uncertainty in the background subtraction.

A $\chi^2$ test[16] of the data indicates that it is consistent with isotropy for both of the observed gamma rays over the energy range studied. The spread expected on the basis of the assigned errors, compared with that observed in the measured anisotropies of the 2.16-Mev radiation, yields $\chi^2/(N-1)=0.7$. The probability ($P$) of $\chi^2/(N-1)$ exceeding this value is 90% if the radiation were isotropic at all energies. This indicates that the assigned errors are somewhat over-generous and that to the precision of the experiment, the radiation is isotropic. Similarly, for the 1.00-Mev radiation $\chi^2/(N-1)=0.8$ and $P=80\%$.

Within the expected errors, the least square mean anisotropies for each gamma ray are equal to each other and to the instrumental anisotropy measured with the $Na^{24}$ source. This is shown in Table IV. The errors indicated do not include systematic errors due to (1) possible misplacement of the $Na^{24}$ source and variations in absorption in target backings ($\pm 0.03$), (2) differences in dead times between the two analyzers ($\pm 0.04$), and (3) differences in efficiencies and absorptions for the different gamma energies involved ($\pm 0.02$).

[14] Obtained from Nuclear-Chicago Corporation, 333 E. Howard Street, Des Plaines, Illinois, and rechecked in our laboratory.

[15] W. F. Miller, J. Reynolds, and W. J. Snow, Argonne National Laboratory Report, ANL-5902 (unpublished).

[16] A. H. Wapstra, G. J. Nijgh, and R. van Lieshout, *Nuclear Spectroscopy Tables* (North-Holland Publishing Company, Amsterdam, 1959), p. 10.

## RESULTS AND CONCLUSIONS

### Cross Sections

Although most of the resonances are only partially resolved, an attempt was made to fit the excitation curves with peaks of half-width equal to the target thickness and, thereby, to estimate the 90-deg peak yield at each resonance. No background subtraction was made, and it was found possible to satisfactorily fit the curves over most of the range without (*ad hoc*) assuming resonances that were not indicated by the data.

Under the assumption that the natural resonance widths are less than the target width, the peak gamma yield at the various resonances can be related to the integral of the cross section over the resonance. This assumption is probably valid for a large majority of the resonances, since they can be fit with a peak shape of the same half-width, i.e., the target thickness.

The further approximation of isotropic gamma emission was made to obtain the total cross section from the measurements at 90°. This is not a bad approximation in the geometry used here, since the crystals subtend a large solid angle and is, in fact, exact for the 1.00-Mev gamma ray and for the 2.16-Mev gamma ray over a large portion of the excitation function to the precision of the measured isotropy.

Table V shows the results of this decomposition of the excitation function. Column 1 lists the resonance energy corrected for the energy loss due to the thickness of the target. The values quoted are considered accurate to ±10 kev absolute and ±5 kev relative. Columns 2 and 4 list the integrated absolute cross sections obtained from the peak gamma-ray yield at resonance for the 1.00-Mev gamma ($\sigma_1$) and the 2.16-Mev gamma ($\sigma_2$), respectively. They were calculated from the expression

$$\int \sigma(E)dE = YSW/AFK,$$

where $Y$ is the measured maximum photopeak yield at resonance per incident proton; $S$ is the stopping power of potassium iodide in Mev cm²/g; $W$ is the molecular weight of potassium iodide; $A$ is Avogadro's number; $F$ is the fraction of $K^{41}$ in the sample, and $K$ is the absolute photo-efficiency of the detector at the relevant energy. Only those resonances with definite observed maxima are listed without question marks. Because of the large uncertainties in the unfolding of the partially resolved resonances, and the expected occurrence of smaller undetected resonances, the cross-section estimates are only considered valid to 50%. From the tabulated values of $\int \sigma dE$, one can obtain the value of the product $\Gamma_T \sigma_R$, where $\Gamma_T$ is the width of the compound state, and $\sigma_R$ is the cross section at the resonance maximum, from the relationship

$$\int \sigma(E)dE = (\pi/2)(\Gamma_T \sigma_R).$$

TABLE V. Properties of states in $Ca^{42}$ near 13-Mev excitation.

| $E_R$ (Mev) | $\int \sigma_1 dE \times 10^{28}$ (Mev cm²) | $\omega\gamma_1$ (kev) | $\int \sigma_2 dE \times 10^{28}$ (Mev cm²) | $\omega\gamma_2$ (kev) | $\Gamma_2/\Gamma_1$ |
|---|---|---|---|---|---|
| 2.321 | 0.2 | 0.008 | 0.2(?)[a] | 0.01 | 1.1 |
| 2.360 | 0.3 | 0.02 | 0.3(?) | 0.02 | 1.1 |
| 2.391 | 0.2 | 0.009 | 0.2(?)[a] | 0.01 | 1.1 |
| 2.457 | [b] | ... | 0.5 | 0.03 | ... |
| 2.494 | 0.2(?)[a] | 0.01 | 0.5[a] | 0.03 | 2.5 |
| 2.507 | 0.9[a] | 0.06 | [b] | ... | ... |
| 2.557 | [b] | ... | 0.7[a] | 0.04 | ... |
| 2.608 | 0.3 | 0.02 | 0.6 | 0.04 | 2.3 |
| 2.619 | 0.2 | 0.01 | 0.4 | 0.03 | 2.3 |
| 2.631 | 0.3 | 0.02 | [b] | ... | ... |
| 2.639 | 0.3 | 0.02 | [b] | ... | ... |
| 2.652 | 0.3 | 0.02 | 0.9 | 0.06 | 3.4 |
| 2.667 | 0.3 | 0.02 | 0.7 | 0.05 | 2.3 |
| 2.680 | 0.3 | 0.02 | 0.3(?) | 0.02 | 1.2 |
| 2.699 | 0.4 | 0.02 | 0.7 | 0.05 | 1.9 |
| 2.709 | 0.3 | 0.02 | [b] | ... | ... |
| 2.720 | 0.4 | 0.03 | [b] | ... | ... |
| 2.724 | [b] | ... | 0.9 | 0.06 | ... |
| 2.731 | 0.6 | 0.04 | [b] | ... | ... |
| 2.746 | 0.5 | 0.03 | 0.3(?) | 0.02 | 0.6 |
| 2.762 | 0.4 | 0.03 | 1.0[a] | 0.07 | 2.6 |
| 2.783 | 0.4 | 0.03 | 0.3(?)[a] | 0.02 | 0.8 |
| 2.797 | 0.4 | 0.03 | 0.6(?)[a] | 0.04 | 1.3 |
| 2.843 | 0.7 | 0.05 | 1.4[a] | 0.09 | 1.9 |
| 2.887 | 0.3 | 0.02 | 1.2 | 0.09 | 4.1 |
| 2.911 | 0.7 | 0.05 | 1.0 | 0.07 | 1.5 |
| 2.922 | 0.6 | 0.04 | 0.5(?)[a] | 0.04 | 0.9 |
| 2.931 | 0.5 | 0.03 | 0.5(?)[a] | 0.04 | 1.1 |
| 2.946 | 0.6 | 0.04 | 0.5(?) | 0.04 | 0.9 |
| 2.962 | 0.5[a] | 0.04 | 0.5[a] | 0.04 | 1.0 |
| 2.989 | 0.8 | 0.06 | [a] | ... | ... |
| 2.996 | [b] | ... | 1.5 | 0.11 | ... |
| 3.018 | 1.5[a] | 0.11 | 1.1[a] | 0.08 | 0.7 |
| 3.063 | 0.9 | 0.06 | 0.9 | 0.07 | 1.1 |
| 3.086 | 1.1 | 0.08 | 0.7[a] | 0.05 | 0.6 |
| 3.115 | 0.6[a] | 0.04 | [b] | ... | ... |
| 3.142 | 2.9[a] | 0.21 | 0.8[a] | 0.06 | 0.3 |
| 3.152 | 1.6(?) | 0.12 | 0.9 | 0.07 | 0.6 |
| 3.176 | 1.1[a] | 0.09 | 1.2[a] | 0.09 | 1.0 |
| 3.195 | 0.9 | 0.07 | 1.0 | 0.08 | 1.1 |
| 3.225 | 1.5[a] | 0.11 | 1.4 | 0.11 | 1.0 |
| 3.262 | 0.8 | 0.07 | [c] | ... | |
| 3.300 | 1.4[a] | 0.11 | [c] | ... | |
| 3.320 | 0.7 | 0.06 | [c] | ... | |
| 3.336 | 1.0 | 0.08 | [c] | ... | |
| 3.369 | 1.0[a] | 0.08 | [c] | ... | |
| 3.389 | 0.9 | 0.07 | [c] | ... | |
| 3.402 | 1.2 | 0.10 | [c] | ... | |
| 3.414 | 1.5[a] | 0.12 | [c] | ... | |

[a] Shape indicates possible unresolved pair. The cross section was estimated for the larger component if only one value is listed.
[b] No indications of resonance observed in this yield curve.
[c] This region obscured in 2.16-Mev yield curve by interfering 1.95-Mev radiation from $K^{41}(p,n)$ and $K^{39}(p,\alpha)$ reactions.
(?) Not a definite differentiated maximum in this yield curve, although curve fitting indicates likely resonance at this energy of approximately the magnitude listed.

The integrated cross section can also be related to the partial widths involved in the reaction

$$\int \sigma(E)dE = \frac{\lambda^2}{16}(2J+1)\frac{\Gamma_p \Gamma_x}{\Gamma_T},$$

where $\lambda$ is the wavelength of the incident proton in the center-of-mass system, $J$ is the total angular momentum of the compound state, $\Gamma_p$ is the partial width for formation of the compound state through the entrance channel, $\Gamma_x$ is the partial width for decay of the com-

pound state through the exit channel, and the numerical factor includes the statistical factor for the target nucleus and incident proton. Therefore, from the tabulated values of $\int\sigma dE$, one can obtain the commonly defined parameter $\omega\gamma$ for the various resonances,

$$\omega\gamma=[(2J+1)/8](\Gamma_p\Gamma_x/\Gamma_T).$$

These values are listed in columns 3 and 5 of Table V. For those resonances observed in both yield curves, the ratio of the measured peak cross sections leads to the partial width ratio for the relative decay probabilities through the two different exit channels, i.e., emission of a proton to the 1.00-Mev state in $K^{41}(\Gamma_1)$, and emission of an alpha particle to the 2.16-Mev state in $Ar^{38}(\Gamma_2)$. This ratio is listed in column 6.

Often in experiments of this type, one of the two partial widths entering the above equations can be shown to be the dominant component of the total width by a calculation of the penetrabilities. In this case, one can calculate $2J+1$ times the smaller partial width from the measured values of $\int\sigma dE$ for the individual resonances, and the average or integral value of the cross section over a large energy region provides information about the strength function. In the energy region of these experiments, however, we are above neutron threshold, and on the basis of the relative penetrabilities involved, the partial neutron width is expected to be an important contributor to the total width. Thus, the individual partial widths and the strength functions cannot be obtained.

## Anisotropies

To calculate the expected anisotropies, we first make the approximation of single isolated compound states and later consider the effects of the breakdown of this assumption. The calculations were made for the case of a triple correlation with the intermediate radiation unobserved, using the tables of Sharp *et al.*[17] Only the lowest allowable orbital angular momenta were considered. Those compound states were chosen which would lead to penetrabilities within an order of magnitude of the most favored situation. The channel spin ratios were calculated assuming pure $jj$ coupling, using the Racah coefficients of Simon, *et al.*[18] The theoretical anisotropies were modified to account for the finite solid angle subtended by the detector by the method of Rose.[19] The $E2$ admixtures to the $M1$ transitions were neglected. The calculated anisotropies and definitions of the notation employed are shown in Table VI. Those situations where the neglected higher orbitals give a contribution within an order of magnitude of the most favored case are indicated. In these cases, interference terms with the higher orbital are most likely to modify the distributions.

TABLE VI. Calculated anisotropies.

Reaction I:

$$K^{41}(\tfrac{3}{2}+)\xrightarrow{R_1,L_1}Ca^{42*}(j_1\pi_1)\xrightarrow{R_{12},L_{12}}K^{41*}(j_2\pi_2)\xrightarrow{R_2,L_2}K^{41}(\tfrac{3}{2}+).$$

Reaction II:

$$K^{41}(\tfrac{3}{2}+)\xrightarrow{R_1,L_1}Ca^{42*}(j_1\pi_1)\xrightarrow{R_{12},L_{12}}Ar^{38*}(2+)\xrightarrow{R_2,L_2}Ar^{38}(0+).$$

$R_i$=type of radiation ($R_1$=proton, $R_{12}$=proton or alpha, $R_2$=gamma). $L_i$=total angular momentum of radiation. $(j_i\pi_i)$=spin and parity of intermediate state. $A=[W(0°)-W(90°)]/W(90°)$. $W(\theta)$=relative intensity of gamma radiation at the angle $\theta$ to the incident beam.

Reaction I: (1.00-Mev radiation)

| $(j_2\pi_2)$ | $(j_1\pi_1)$ | $L_1$ | $L_{12}$ | $A$ |
|---|---|---|---|---|
| $\frac{1}{2}+$ | 0+, 1+, 2+<br>0−, 1−, 2− | ... | ... | 0 |
| $\frac{3}{2}+$ | 1+ | ... | ... | 0[a] |
| | 2+ | ... | ... | 0[a] |
| | 0− | ... | ... | 0 |
| | 1− | $\frac{1}{2}$ | $\frac{1}{2}$ | 0 |
| | | $\frac{1}{2}$ | $\frac{3}{2}$ | 0 |
| | | $\frac{3}{2}$ | $\frac{1}{2}$ | +0.27 |
| | | $\frac{3}{2}$ | $\frac{3}{2}$ | +0.19 |
| | 2− | ... | ... | 0 |
| | 3− | ... | ... | +0.30 |
| $\frac{5}{2}+$ | 1+ | ... | ... | 0 |
| | 2+ | ... | ... | 0[a] |
| | 3+ | $\frac{3}{2}$ | $\frac{1}{2}$ | −0.31 |
| | | $\frac{5}{2}$ | $\frac{1}{2}$ | −0.25 |
| | 1− | $\frac{1}{2}$ | $\frac{3}{2}$ | 0 |
| | | $\frac{3}{2}$ | $\frac{3}{2}$ | +0.17 |
| | 2− | ... | ... | 0 |
| | 3− | $\frac{3}{2}$ | $\frac{1}{2}$ | −0.31 |
| | | $\frac{3}{2}$ | $\frac{3}{2}$ | −0.18 |
| $\frac{7}{2}+$ | 1+ | ... | ... | 0 |
| | 2+ | ... | ... | 0 |
| | 3+ | $\frac{3}{2}$ | $\frac{1}{2}$ | +0.51 |
| | | $\frac{5}{2}$ | $\frac{1}{2}$ | +0.43 |
| | 4+ | ... | ... | +0.65 |
| | 2− | ... | ... | 0 |
| | 3− | $\frac{3}{2}$ | $\frac{1}{2}$ | +0.51 |
| | | $\frac{3}{2}$ | $\frac{3}{2}$ | +0.33 |

Reaction II: (2.16-Mev radiation)

| $(j_1\pi_1)$ | $L_1$ | $A$ |
|---|---|---|
| 1+ | ... | 0 |
| 2+ | ... | 0[a] |
| 1− | $\frac{1}{2}$ | 0 |
| | $\frac{3}{2}$ | −0.26 |
| 2− | ... | 0 |
| 3− | ... | +0.59 |

[a] Neglected higher orbitals most likely to contribute.

The 2.16-Mev gamma radiation originates in a state of known spin (2+) in $Ar^{38}$ so that the only parameters in the calculation are the spin and parity of the compound state $(j_1\pi_1)$ and the total angular momentum of the incident proton $(L_1)$. The calculated anisotropies for the various assumed values of these parameters are plotted in Fig. 6(b) along with the experimental results. It is seen that under the assumptions noted, it is unlikely that there are any 3− or 1− ($L_1=\frac{3}{2}$) states with large cross sections in the regions of excitation of $Ca^{42}$ that

[17] W. T. Sharp, J. M. Kennedy, B. J. Sears, and M. G. Hoyle, Atomic Energy of Canada Limited Report, CRT-556, 1954 (unpublished).

[18] A. Simon, J. H. Vander Sluis, and L. C. Biedenharn, Oak Ridge National Laboratory Report, ORNL-1679, 1954 (unpublished).

[19] M. E. Rose, Phys. Rev. **91**, 611 (1953).

were studied. The observed states can be 1+, 2+, 1− ($L_1=\frac{1}{2}$), or 2− within the penetrability limits indicated.

The 1.00-Mev gamma radiation originates in a state of unknown spin in $K^{41}$. From the previously known information about the low-lying states of this nucleus, we can estimate the most likely range of values for the spin and a parity of the 1.00-Mev state as follows. The ground state has been measured to be $\frac{3}{2}+$, and is probably of the $(d_{3/2})^{-1}[(f_{7/2})^2]_0$ configuration. The 1.29-Mev state has been measured as $\frac{7}{2}-$ from the decay of $Ar^{41}$, and is probably of the $[(d_{3/2})^{-2}]_0[(f_{7/2})^3]_{7/2}$ configuration. This configuration is expected to correspond to the lowest lying negative parity state. The 1.00-Mev state, therefore, is probably positive, and is most likely one of those states expected from the $(d_{3/2})^{-1}[(f_{7/2})^2]_2$ configuration.[20]

The fact that neither the $\beta$ decay from a $[(d_{3/2})^{-2}]_0\times[(f_{7/2})^3]_{7/2}$ configuration in $Ar^{41}$, nor the $(dn)$ reaction from a $[(d_{3/2})^{-2}]_0[(f_{7/2})^2]_0$ configuration in $Ar^{40}$ goes to the 1.00-Mev state, while both are observed going to the higher 1.29-Mev state, supports this hypothesis, since in both cases a core rearrangement would be necessary to go to the former, but not to the latter. If this is indeed the configuration of the 1.00-Mev state, the possible spins are $\frac{1}{2}$, $\frac{3}{2}$, $\frac{5}{2}$, and $\frac{7}{2}$. The anisotropies for each of these spins were calculated under the assumptions previously indicated. In Fig. 5(b), they are plotted along with the experimental results.

It is seen that a likely explanation for the observed isotropy is that the spin of the 1.00-Mev state is $\frac{1}{2}+$, although, because of the large experimental uncertainties, this is by no means certain. If, for example, one assumes that many of the same states are excited in each reaction, as seems reasonable from the correspondence in energies, then in the energy region up to about 3.25 Mev, one can say from the 2.16-Mev results that 3− and 1− ($L_1=\frac{3}{2}$) states are not found anyway; and the assumption of spin $\frac{3}{2}$ for $j_1$ becomes as likely as $\frac{1}{2}$. However, the isotropy in the case of $j_1=\frac{1}{2}$ is due to a general rule and remains even under the breakdown of the poor approximation of isolated compound states. The "accidental" isotropies calculated for the other hypothetical spins are dependent on this and the assumption that no higher orbital angular momenta enter (a poor assumption for those states indicated in Table VI). Thus, any breakdown of these assumptions strengthens the likelihood of the assignment $\frac{1}{2}+$.

Also, in the region above 3.25 Mev we have eight more resonances for the 1.00-Mev radiation where there are no restrictions on the spins from the 2.16-Mev measurements, and, therefore, no reason not to expect anisotropies in the 1.00-Mev radiation unless $j_1=\frac{1}{2}$. Therefore, it is felt that the observed isotropy of the 1.00-Mev radiation does indicate that the most likely assignment for this level is $\frac{1}{2}+$.

This assignment is in agreement with the predictions of Pandya.[3] Based on a $jj$-coupling shell model and the positions of low-lying states in adjoining nuclei, he calculates the excitation energy of a $\frac{1}{2}+$ level of the $(d_{3/2})^{-1}(f_{7/2})^2$ configuration to be 1.00 Mev in $K^{41}$.

## Average Level Spacing

If one assumes that the levels in the compound nucleus are positioned randomly, it can be shown that the distribution function for the spacings is given by $P(x)=e^{-x}$, where $x=S/D=$spacing/mean spacing, and $P(x)$ is the probability distribution for a spacing having a value between $x$ and $x+dx$. Recently, Wigner has proposed that for levels of the same spin and parity the spacings distribution should be given to a good approximation by $P(x)=(2\pi x)^{-1}\exp(-\frac{1}{4}\pi x^2)$, which corresponds to a reduced number of small spacings. This "level repulsion" has been observed experimentally.[21]

As the number of families of compound states of the same spin and parity increases, the distribution in spacings varies from the Wigner distribution to the exponential. Under the approximation that they each have the same average spacing, the distribution of level spacings for five or more families of compound states is represented to a good approximation by the exponential distribution. A calculation of the barrier-penetration coefficients for the reactions considered here (assuming spin $\frac{1}{2}+$ for the 1.00-Mev state) shows that the transmission coefficients are within an order of magnitude for the excitation of compound states of spin 1+, 2+, 1−, 2−, and 3− in the 2.16-Mev excitation function, and for compound states of spin 0+, 1+, 2+, 0−, 1−, and 2− for the 1.00-Mev excitation function. Therefore, the approximation of an exponential distribution of level spacings about their average value was considered justifiable.

In general, one expects a distribution in resonance sizes as well as a distribution in spacings. This size distribution can be related to the distributions in reduced partial widths involved in the reaction. For a given family of compound states of the same spin and parity, these partial-width distributions have been found to be roughly exponential in character.[22]

We are missing resonances in our experimental observations because of their small sizes and close spacings to other resonances. We will approximate these effects by assuming cutoffs at some minimum spacing ($S_{\min}$) and size ($Y_{\min}$) in the distributions.

First consider the spacing distribution as it would be

[20] Since the 2+ first-excited state in $Ca^{42}$ is probably $(f_{7/2}^2)_2$, one expects this configuration to be low lying in $K^{41}$.

[21] See N. Rosenzweig and C. E. Porter [Phys. Rev. **120**, 1698 (1960)] and the references cited therein for an analysis of the distribution of level spacings in nuclei.

[22] A distribution of the form $x^{-\frac{1}{2}}\exp(-\frac{1}{2}x)$ has been shown to fit best the observed distributions of neutron reduced widths, where $x$ equals a particular value of the reduced width divided by the average value for levels of that spin and parity. See also references 6 and 7.

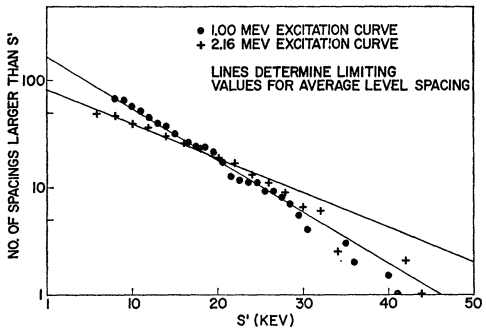


FIG. 7. Integral spacings distribution of levels in $Ca^{42}$. The number of level spacings larger than $S'$ from the 1.00-Mev and 2.16-Mev excitation curves. Upper limits on the average level spacing ($D'$), corresponding to the lines drawn through the points, are obtained from the slope and intercept of each line. For the 1.00-Mev curve: $D'$ (slope) $\leqslant 9$ kev, $D'$ (intercept) $\leqslant 7$ kev. For the 2.16-Mev curve: $D'$ (slope) $\leqslant 14$ kev, $D'$ (intercept) $\leqslant 12$ kev.

observed with infinitely good resolution and sensitivity

$$N(S)=(N_T/D)e^{-S/D},$$

where $N(S)$ is the number of spacings between $S$ and $S+dS$, $N_T$ is the total number of spacings in the energy region $\Delta E$, and $N_T=\Delta E/D$. If this were a good approximation to the observed spacing distribution, one could plot the logarithm of the observed distribution and obtain the average spacing $D$ from the slope of the best linear approximation to the data or from its total integrated area $N_T$.

The effects of finite resolution and sensitivity will distort the observed distribution from the one given above. It will be shown, however, that the procedure outlined will result in an upper limit to the average level spacing.

First, consider the effects of finite sensitivity only. We remove from the above distribution all those resonances whose size is below some cutoff, $Y_{\min}$. If the size and spacing distributions are independent,[23] the remaining resonances are still randomly spaced and, therefore, exponentially distributed. There are fewer spacings, however, and the average spacing is therefore larger. The exponential distribution will, therefore, be lowered in normalization and have an increased decay length. Let $N_T'$ be the total number of resonances in the new distribution $N(S')$.

$$N(S')=N_T'e^{-S'/D'}/D',$$

where $D'$ is the average level spacing of $N_T'$ resonances larger than $Y_{\min}$. ($N_T'<N_T$ and $D<D'$.)

Now consider the effects of finite resolution. To a first approximation they can be represented as a cutoff in the $S'$ distribution at some $S_{\min}'$. To this approximation an extrapolation of the observed $S'$ distribution back to the origin should give $N_T'$, which is certainly a lower limit on the total number of levels $N_T$. An upper limit on the average level spacing could therefore be obtained from the relation $D'=\Delta E/N_T'$, and the same $D'$ should be obtained from the slope of the logarithm of the $N(S')$ distribution in the observed regions $S'>S_{\min}'$.

Let us further consider the effects of finite resolution. To a second approximation, when two resonances are unresolved their sizes become partially additive. Thus, some smaller resonances, which were below the cutoff, become observable. These effects can be represented by a lowering of $Y_{\min}$ to some effective $Y_{\min}'$. The previous considerations should still be valid, however. A further effect of those spacings, unobserved because they are smaller than $S_{\min}'$, is to increase the size of the adjoining spacings (assuming that the spacings are measured from the centers of the composite peaks). Thus, the value of $D'$ obtained from the slope of the logarithm of the observed distribution is going to be larger than expected from considering the effects of $Y_{\min}'$ only. The estimate of $N_T'$ obtained from the extrapolation is still a lower limit on the total number of resonances, but will result in a somewhat smaller $D'$ than obtained from the slope, since one is in effect "putting back" some of the resonances missed due to their small spacing, and estimating, to a first approximation, the effects of $Y_{\min}'$ alone. Thus, the value of $D'$ obtained from the quotient $\Delta E/N_T'$ should give the best limit.

These considerations are illustrated in Fig. 7, where, to minimize statistical fluctuations, we have plotted the integral distribution; namely, the number of observed spacings greater than some $S'$ as a function of $S'$, $M(S')$.

$$M(S')=N_{T'}\int_{D'}^{\infty}\frac{e^{-S'/D'}}{D'}dS'=N_{T'}e^{-S'/D'}.$$

The slope of the logarithm of the integral distribution should be the same, and $N_T'$ is now obtained from the extrapolated ordinate at $D'=0$. Otherwise, all the previous considerations still hold.

The result of this procedure is upper limits of 7 kev on the average level spacing observed in the 1.00-Mev excitation curve and 12 kev for the 2.16-Mev excitation curve.

Now, let us compare our observed limits for the average level spacing with the predictions of the semiempirical formulas based primarily on slow-neutron data.[4,5] Evaluation of Newton's formula yields about 12 kev as the average level spacing for $J=0$ levels in $Ca^{42}$ at this excitation. We assume that those compound states, whose penetrabilities are down by an order of magnitude from the most favored, are not appreciably excited. Then in the 2.16-Mev gamma excitation function we should expect $1+$, $2+$, $1-$, $2-$, and $3-$ states to be formed and the average level spacing, using Cameron's corrected $J$ dependence (1959) becomes

[23] J. A. Harvey and J. D. Hughes [Phys. Rev. **109**, 471 (1958)] have shown that for the reduced neutron widths and spacings in $U^{238}$ the two distributions are independent. This is assumed to hold for the situation considered here.

$D=0.8$ kev. [We have here included 3− and 1− ($L_1=\frac{3}{2}$) states even though they appear to be absent in that portion of the excitation function for which anisotropy measurements were made. Leaving out 3− and 1− states completely yields a $D=1.4$ kev.] For the 1.00-Mev excitation function, including those compound states whose penetrabilities are within an order of magnitude (0−, 1−, 2−, 0+, 1+, 2+), we obtain similarly a predicted average level spacing of $D=0.9$ kev.

It is seen that the predictions of the model are an order of magnitude smaller than our observed upper limits. However, one does not expect to see all the resonances of the families of compound states listed above, but only those at the high end of the size distribution. The experiments are only imcompatible with the theory if the small average spacing required by the theory would necessarily mean the washing out of the structure of the excitation function. This is difficult to say without a detailed knowledge of the distribution of resonance sizes among the compound states considered. If the distribution is steep enough, it is possible that even the large number of resonances required by the theory would not appreciably wash out the structure. The resonance size distribution is not simply related to the Porter-Thomas distribution expected for individual reaction widths, since several reaction widths enter the expression for the cross section, and several families of compound states of different spins and parities are expected to be excited. It is, however, most likely that the distribution rises sharply for small sizes, and a significant number of resonances are unobserved. Therefore, the most that can be said is that these findings are not obviously inconsistent with the predictions of the semiempirical theory.

If, however, the average level spacing were indeed this small, one might question the results of the analysis of the anisotropy measurements. If the interference terms in the angular distributions, due to these many small resonances, are enough to wash out the structure in the angular distributions, even though the intensity of these resonances is not large enough to wash out the structure in the excitation curve, then one could explain the observed isotropy by saying that we were in the "statistical region" for angular distribution measurements, but not for excitation function measurements. This is certainly a possibility; however, we consider it less likely than the alternative conclusions of the previous section.

## SUMMARY

The results of these experiments can be summarized as follows: (1) The energy measurement and identification of some of the gamma radiation following the proton bombardment of potassium as proceeding from the $K^{41}(p,p'\gamma)$ and $K^{41}(p,\alpha\gamma)$ reactions. (2) The determination of the energies and absolute cross sections of approximately 50 resonances corresponding to excited states in $Ca^{42}$ near 13-Mev excitation, and the tabulation of some of the resonance parameters. (3) Anisotropy measurements leading to restrictions on the spins of the compound states excited in $Ca^{42}$ and to the likelihood of the 1.00-Mev state being $\frac{1}{2}+$. (4) An upper limit on the average level spacing, in $Ca^{42}$, which is an order of magnitude larger than predicted by the semiempirical theory, possibly accountable for by the missing of a large number of very small resonances.

## ACKNOWLEDGMENTS

We would like to acknowledge the help of L. D. Singletary with the many calculations involved in the analysis of the data; A. J. Meyerott for assistance in the design of the vacuum apparatus; and J. H. Rowland for his measurement of the spectrometer efficiency. We would like to thank Martin Walt for his comments on, and criticisms of the manuscript.